Amorphous-amorphous transformation induced in glasses by intense x-ray beams

E. Alfinelli [1,*] F. Caporaletti,[2,3] F. Dallari [4] A. Martinelli [5] G. Monaco [5] B. Ruta,[6,7] M. Sprung,[4]
M. Zanatta [1] and G. Baldi [1]

[1]*Physics Department, University of Trento, I-38123 Povo, Trento, Italy*
[2]*Van der Waals-Zeeman Institute, Institute of Physics, University of Amsterdam, 1098XH Amsterdam, The Netherlands*
[3]*Van't Hoff Institute for Molecular Sciences, University of Amsterdam, Science Park 904, 1098XH Amsterdam, The Netherlands*
[4]*Hasylab at DESY, Notkestraße 85, D-22607 Hamburg, Germany*
[5]*Physics and Astronomy Department, University of Padova, I-35122 Padova, Italy*
[6]*ESRF–The European Synchrotron, F-38043 Grenoble, France*
[7]*Institut Lumière Matière, UMR5306 Université Lyon 1-CNRS, Université de Lyon, 69622 Villeurbanne Cedex, France*

The atomic displacements induced by an x-ray beam of relatively low energy, $\epsilon \sim 8$ KeV, are investigated in pure boron oxide and in a set of sodium silicate glasses by means of x-ray photon correlation spectroscopy. We observe the complete x-ray induced transformation of the initial glass into a new amorphous state which remains stable under irradiation. The new phase continues to rearrange under the beam with a stretched exponential relaxation similar to the one observed with macroscopic measurements in the corresponding high-temperature supercooled liquid, suggesting that the new configuration lies in a higher energy minimum of the potential energy landscape. We investigate the temperature dependence of the observed dynamics for a specific sodium concentration and we observe a temperature dependence of the beam induced motion, which suggests that the defect creation rate is thermally activated. The radiation dose needed for the initial structural variation is sample dependent and correlates well with the number of constraints per vertex, within the framework of rigidity theory. This observation provides a quantitative tool to evaluate the efficiency of the radiolytic process in different network topologies.

I. INTRODUCTION

The common way to produce a glass is by quenching the melt at a sufficiently high cooling rate. The resulting solid material lies in an out-of-equilibrium state corresponding to a deep minimum of the potential energy landscape (PEL) [1]. Irradiation of several ceramic materials with nuclear or ionizing radiation represents an alternative route to glass formation [2,3]. The initially crystalline state is transformed to an amorphous phase at sufficiently high radiation doses. Neutrons, fast ions, highly energetic electrons, or γ-rays can induce the direct knock-on displacement of atoms from their equilibrium position [4]. Less energetic particles, such as electron beams in a scanning electron microscope or UV laser radiation, can generate permanent atom displacements as a consequence of electronic excitations during the radiolytic process [5,6]. Irradiation of pure vitreous silica with neutrons or heavy ions leads to a final amorphous state which is denser by a few percent with respect to the pristine glass. The irradiated glass is believed to be the same phase that can be obtained starting from the crystal [7]. The evolution of crystalline α-quartz under irradiation with fast neutrons has been recently investigated by numerical simulations [8]. The amorphized quartz is seen to lie in a higher energy region of the landscape with respect to the normal glass, and with

a structure presenting a ring size distribution similar to that of a hyperquenched glass.

The continuous increase of the energy density of x-ray beams produced at synchrotron radiation sources has opened the possibility to observe the atomic motion induced by the radiolytic process in several glasses [9–15]. The technique of x-ray photon correlation spectroscopy (XPCS) is a natural choice to probe the density fluctuations at interatomic distances and it is sensitive to beam induced atomic displacements. The intermediate scattering function of supercooled liquids is well described by a stretched exponential, or Kohlrausch-Williams-Watts (KWW) function [16,17], $F(Q, t) \sim e^{-(t/\tau_\alpha)^\beta}$, where τ_α is the structural relaxation time and $0 < \beta < 1$. The beam induced dynamics in vitreous silica and vitreous germania shows a peculiar compressed, or faster than exponential, shape with $\beta > 1$ [10]. A similar dynamical signature has been reported during the aging of soft solids [18] and by XPCS in metallic glasses [19,20]. In soft matter it has been interpreted as the signature of a dynamics that proceeds through the release of stress accumulated inside the material, via the rupture of network connections [21,22]. The beam induced dynamics is observed also in other oxide glasses such as boron oxide [13,15], alkali borates [12,14,23], and silicates [9], where the correlation curves can be well described by the normal stretched exponential function ($\beta \leqslant 1$).

The investigations reported so far have been limited to absorbed doses of a few gigagray. The x-ray beam rearranges the scattering volume with an induced relaxation time, τ_{ind},

*erica.alfinelli@unitn.it

inversely proportional to the absorbed photon flux. At low temperatures the intrinsic structural relaxation is hidden by this artificial dynamics and becomes measurable only at high temperatures, when τ_α is comparable to the τ_{ind} imposed by the photon beam. The peculiar dynamics of the beam irradiated glass appears related to the network topology, as recently observed in a family of alkali borates [23]. The induced relaxation time, τ_{ind}, corresponds to the radiation dose necessary for the complete rearrangement of the glass configuration, since the XPCS correlation function is a collective property of the system and it decorrelates completely at times longer than τ_{ind}. The XPCS technique is more sensitive to the effect of radiation than the static structure factor, since we can observe complete decorrelation of the intermediate scattering function even at absorbed doses where the first sharp diffraction peak (FSDP) of the glass is barely affected [10]. Moreover, the absorbed dose associated to τ_{ind} is very different in different glasses. Specifically, in vitreous silica this quantity is approximately two orders of magnitude higher than in pure boron oxide, and this difference has remained unexplained [10,13].

Hobbs and co-workers [24,25] have shown that the dose necessary for the amorphization of many crystalline ceramic oxides under heavy ion irradiation correlates well with the number of constraints per vertex as determined in the rigidity theory of Cooper and Gupta [26]. This version of the rigidity theory differs from the one developed by Phillips [27] because it identifies the polytope as the elementary constituent of the network instead of imposing the constraints at the level of single bond lengths and bond angles. The theory finds a geometrical solution to the question of the existence of infinitely large topologically disordered (TD) networks, if the polytopes can be unambiguously identified. The natural choice of the polytope for silicon dioxide is the tetrahedron. Irradiation has the effect to break some of the vertices between the tetrahedra, allowing the structure to rearrange. Both crystalline α-quartz and vitreous silica evolve towards a similar metamict phase. The final amorphous configuration still has tetrahedral coordination but the medium range order is different from that of the normal glass, as evidenced by a significant variation of the first sharp diffraction peak [2,4].

Here we report on a detailed investigation of the beam induced dynamics in pure boron oxide and in a series of sodium silicate glasses. The present study is performed in the new amorphous phase, at absorbed doses of a few gigagray and above, to investigate the connection between the dose required to undergo the amorphous-amorphous transformation and the one corresponding to the continuous rearrangement under x-ray illumination. We show that a proper evaluation of the network rigidity can quantitatively explain the difference in dose required to induce the amorphous-amorphous transformation in a selection of glasses ranging from pure boron oxide to pure silicon dioxide and including the sodium silicates of the present investigation. Moreover, we study in some detail the temperature dependence of the dynamics of the silicate sample with the highest sodium content. In this sample the radiation does not cause an appreciable variation of the static structure factor, while the beam induced dynamics is present and persists even above the glass transition temperature. We show that the peculiar temperature dependence of this process, which is qualitatively different from that previously observed

in borate glasses [13], can be attributed to the thermally activated nature of the defect creation rate.

The paper is organized as follows. In Sec. II we give details on the sample preparation, on the x-ray photon correlation spectroscopy experiment and on the data analysis. In Sec. III we present and discuss the results. We investigate the dose dependence at room temperature of the structure and dynamics of the studied glasses in Sec. III A; the temperature evolution of the silicate sample with 43% of sodium oxide is explored in Sec. III B; the relationship between the beam induced dynamics at room temperature and that of the corresponding high temperature liquid is discussed in Sec. III C; Sec. III D is devoted to the connection between the network rigidity and the dose necessary for the structural and dynamical evolution. Final remarks and conclusions are drawn in Sec. IV.

II. EXPERIMENT AND DATA ANALYSIS

A. Samples

The chosen samples for this study are pure B_2O_3 and $(Na_2O)_x(SiO_2)_{(1-x)}$ at $x = 16\%$, 20%, 23%, and 43%. In what follows the silicate samples are labeled in terms of their Na_2O concentration: Na16, Na20, Na23, and Na43, respectively. The sodium silicate glasses have been prepared starting with silica and sodium carbonate powders melted in a crucible of a refractory material at a temperature well above their melting point. This allowed us to obtain perfectly transparent samples.

Pure B_2O_3 has been prepared in a similar way, by melting the corresponding powder in an alumina crucible at $1000\,°C$. The liquid has been kept at constant temperature for 5 days to remove residual air bubbles and then quenched on metallic plates kept at a temperature of $200\,°C$. The sodium oxide concentration of the four silicate samples has been verified by energy dispersive x ray in a scanning electron microscope and the approach has an overall uncertainty of $\sim1\%$. Cylindrical specimens of a few millimeters in diameter were optically polished to reach the wanted thickness, a trade-off between good XPCS contrast and reasonably high scattered intensity. Measured values of the thickness obtained from x-ray transmission are reported in Table I together with other relevant physical properties.

B. X-ray photon correlation spectroscopy

The data have been collected during two different experiments, both performed at beamline P10 of the Petra III synchrotron in Hamburg, Germany. More in detail, samples

TABLE I. Relevant physical properties of the investigated samples. The attenuation length is calculated at the energy of the XPCS x-ray beam: $\epsilon = 8.25$ KeV for the Na20 and Na43 samples (highlighted in gray) and $\epsilon = 8.4$ KeV for B_2O_3, Na16, and Na23.

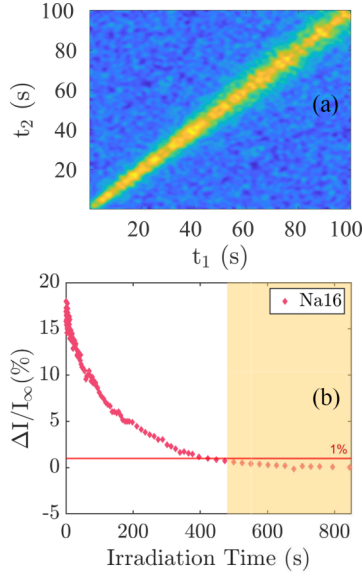| Sample	B_2O_3	Na16	Na20	Na23	Na43
Thickness (μm)	51(3)	43(2)	49(5)	56(5)	46(1)
Density (g/cm³) [28]	1.84	2.35	2.38	2.40	2.545
Attenuation length (μm) [29]	745.0	148.8	140.8	149.0	143.1
T_g (K) [30]	560	780	750	720	670

FIG. 1. Evolution of the dynamics (upper panel) and of the structure (lower panel) of the Na16 sample as a function of the irradiation time at room temperature and $Q = 1.56$ Å^{-1}. (a) Two times correlation function at relatively low absorbed doses. (b) Evolution of the first sharp diffraction peak intensity as a function of exposure time. The shaded area (yellow) is the temporal window used to calculate the $g^{(2)}$ function.

Na20 and Na43, highlighted in gray in Table I, have been investigated during experiment number I-20180946 while Na16, Na23, and B_2O_3 have been studied in experiment number I-20190834. The transversely coherent portion of the x-ray beam with an energy $\epsilon \sim 8$ KeV (8.25 keV for I-20180946, 8.4 keV for I-20190834) is focused to a spot with FWHM $\sim 3 \times 2$ μm^2 (3×2 μm^2 for I-20180946, 1.9×2.7 μm^2 for I-20190834) with a constant photon flux $\phi \sim 5 \times 10^{10}$ ph/s (4.2×10^{10} ph/s for I-20180946, 5.7×10^{10} ph/s for I-20190834). The value of the incident flux was measured for each experiment by means of a calibrated pin diode [31]. The speckle pattern is collected by an EigerX4M detector single-photon counter with 75×75 μm^2 pixel size and a maximum frame rate of 750 Hz. The detector is placed 1.8 m downstream from the sample to match the speckle and the pixel sizes. The microscopic dynamics is calculated from the autocorrelation of the scattered intensity, using a multispeckle approach that allows us to investigate out-of-equilibrium and nonergodic systems [32]. The method exploits an average over many coherence areas to allow for a reliable determination of the temporal average even when the characteristic timescale of the observed process is of the same order of magnitude of the total measuring time. We have divided the area of the EigerX4M detector into three regions of interest (ROI) to get a higher Q resolution, of the order of $\delta Q/Q \sim 5\%$. The two times correlation function (TTCF) is defined as follows:

$$G(Q, t_1, t_2) = \frac{\langle I_p(t_1) I_p(t_2) \rangle_p}{\langle I_p(t_1) \rangle_p \langle I_p(t_2) \rangle_p}, \quad (1)$$

where $\langle \cdots \rangle_p$ is the average over pixels within the chosen ROI. An example of a TTCF for the Na16 silicate sample is shown in the upper panel of Fig. 1.

The TTCF gives information on the time evolution of the dynamics observed by means of XPCS. In the specific example of the Na16 sample, the beam induced dynamics is time dependent, as indicated by the progressive broadening of the diagonal of the TTCF map (Fig. 1, upper panel). In other words, the relaxation time, τ, of this process shows a dependence on the total absorbed radiation dose. This kind of induced "aging" takes place in parallel with a reduction of the first sharp diffraction peak intensity. The relative variation of the FSDP is shown for Na16 in the lower panel of Fig. 1 and indicates a transformation from the initial glass structure to a new configuration that is stable under irradiation. A similar aging of the dynamics with exposure time is observed in the boron oxide glass, while silicates at higher Na concentrations show the opposite trend, with a relaxation time decreasing at higher absorbed doses. We computed the XPCS autocorrelation function for all the studied samples from the temporal average of the TTCF in the region where the FSDP intensity is stable to irradiation, after the completion of the structural transformation. More specifically, we fixed a threshold at 1% of the final intensity and integrated the TTCF from that point onwards to obtain the XPCS autocorrelation function $g^{(2)}(Q, t)$:

$$g^{(2)}(Q, t) = \langle G(Q, t_0, t_0 + t) \rangle, \quad (2)$$

where $\langle \cdots \rangle$ represents the temporal average and t_0 is the time corresponding to the chosen threshold. The interval for the temporal average is highlighted by the shaded area in the lower panel of Fig. 1.

III. RESULTS AND DISCUSSION

A. Radiation induced amorphous-amorphous transformation

Some examples of correlation curves are reported in Fig. 2, together with the best fitting function adapted to the following model, based on the Siegert relation:

$$g^{(2)}(Q, t) = y_0 + \mathcal{C}_Q |F(Q, t)|^2. \quad (3)$$

Here y_0 is a baseline, with a value close to 1, $\mathcal{C}_Q$ is the experimental contrast, and $F(Q, t)$ is the intermediate scattering function, which can be approximated by the KWW relation:

$$F(Q, t) = f_Q e^{-(t/\tau_Q)^{\beta_Q}}. \quad (4)$$

In the expression, f_Q is the nonergodicity factor, τ_Q is the decay time typical of the investigated dynamics, and β_Q is the stretching parameter. The high quality of the correlation curves is well visible even if those have been calculated from a single measurement for every sample. At room temperature the x-ray beam induces a complete decorrelation of the XPCS curves for all the investigated samples, as shown in panels (a) and (b) of Fig. 2. The relaxation time of the beam induced dynamics is of the order of 10–20 s in all the studied samples at the photon flux density used in the present experiment. As discussed in the Introduction, this quantity is more properly expressed as the absorbed dose necessary for the complete rearrangement of the atomic configuration in the glass. We define the absorbed dose (energy per atom) associated to the
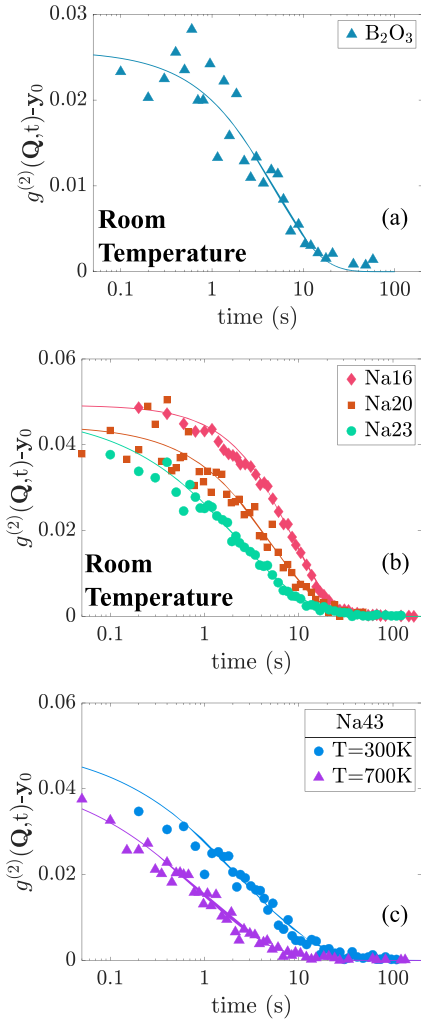
FIG. 2. XPCS correlation curves at $Q = 1.56$ Å^{-1}. Panel (a): data at room temperature for boron oxide. The line is the best fitting function to the KWW model of Eq. (3), with parameters $\tau = (11.0 \pm 0.9)$ s and $\beta = 0.8 \pm 0.1$. Panels (b) and (c) refer to the silicate glasses. Panel (b) shows the room temperature data for the sodium silicates at the three sodium oxide concentrations indicated in the legend. Panel (c) shows the curves for Na43 at two temperatures. The KWW fits are shown as continuous lines and the corresponding parameters are discussed in the text.

beam induced relaxation time, τ_{ind}, as

$$D = \frac{F \epsilon \tau_{\text{ind}}}{N}, \qquad (5)$$

where N is the number of atoms in the scattering volume, ϵ is the beam energy, and F is the absorbed photon flux, defined as $F = \phi(1 - T_r)$, with T_r the sample transmission and ϕ the incident photon flux. The scattering volume is calculated by considering the area of the focal spot as an ellipse with semiaxes the 2-σ value of the Gaussian beam, equal to FWHM$\sqrt{2 \log_e 2}$. The absorbed dose of the beam induced dynamics for boron oxide is considerably smaller than the one necessary for the silicate samples, even if τ_{ind} is comparable, because the sample transmission is higher. We will discuss this point in more detail in Sec. III D. Considering the silicate glasses, an increase in the sodium content implies
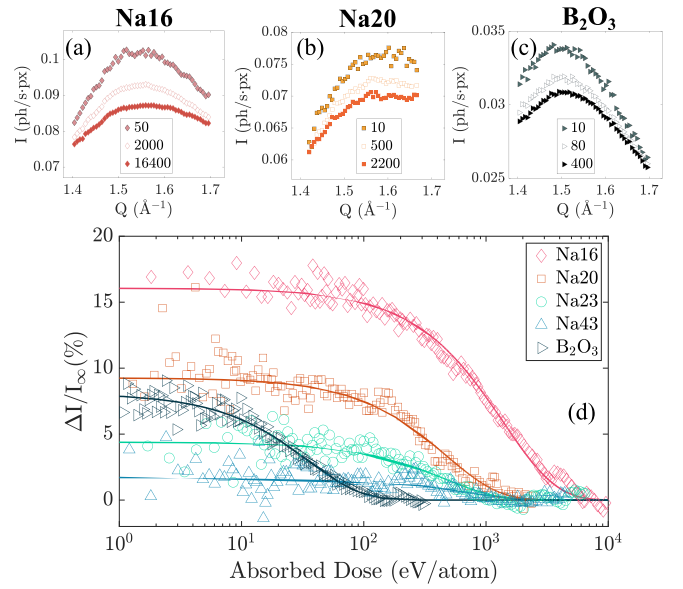

FIG. 3. (a)–(c) Partial diffraction pattern for samples Na16, Na20, and B$_2$O$_3$, respectively, at the indicated doses (eV/atom). These represent three stages of the irradiation phenomenon: no intensity variation (low dose profile, dots with black edges), during the amorphous transformation (empty dots), and when the transformation is complete (high dose profile, colored dots). (d) FSDP intensity as a function of the absorbed dose in the investigated samples. The intensity is plotted as relative variation with respect to the intensity at high doses, I_∞ (see text). The continuous lines are the best fitting functions to the simple exponential model of Eq. (6). The intensity I is calculated as the integral over the wave-vector region between 1.5 and 1.6 Å^{-1}, while the entire Q range covered by the detector is shown in panels (a)–(c).

a reduction of the relaxation time and a change in shape of the correlation curve corresponding to a reduction of the β parameter, as shown in panel (b) of Fig. 2. The lower panel of the figure shows the $g^{(2)}$ function at two temperatures for the Na43 sample. A temperature increase induces a reduction of the relaxation time, without a significant variation of the shape of the curve.

Absorption of a sufficiently high x-ray dose induces the transformation to a new amorphous state, in the glasses under study. The transformation is visible in the diffraction pattern as a decrease of the intensity of the FSDP at 1.5 Å^{-1} which tends to a constant value at high absorbed doses. The dose dependence of the FSDP intensity, I, can be fitted to the following exponential function:

$$I = I_\infty + (I_0 - I_\infty)e^{-d/D_I}, \qquad (6)$$

where I_0 and I_∞ are, respectively, the initial and final FSDP intensities, d is the absorbed dose at exposure time t, and D_I is the absorbed dose necessary for the structural transformation. The required dose for the transformation to the new amorphous state in boron oxide is significantly smaller than that for the silicate glasses, as shown in Fig. 3, with a trend analogous to the absorbed dose associated to the beam induced dynamics. The quantity plotted in the figure is the relative variation of the intensity with respect to its final value, $\Delta I/I_\infty = (I - I_\infty)/I_\infty$. Within the set of silicate
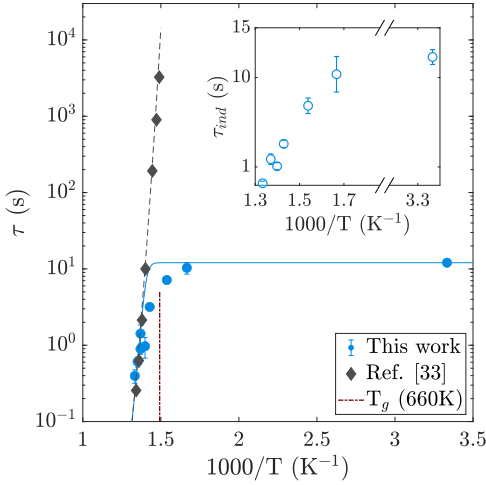
FIG. 4. Arrhenius plot of the relaxation time measured with XPCS (circles) for the Na43 sample at $Q = 1.5$ Å^{-1}, together with the macroscopic equilibrium value of the structural relaxation from the frequency dependence of the loss modulus [33] (black diamonds). The dashed gray line is a fit to the VFT model. The continuous line is obtained from Eq. (7) assuming a T-independent τ_{ind} and using the VFT fit for τ_α. Inset: temperature dependence of τ_{ind}. The data are relative to the following temperatures: 750, 730, 715, 700, 650, 600, and 300 K.
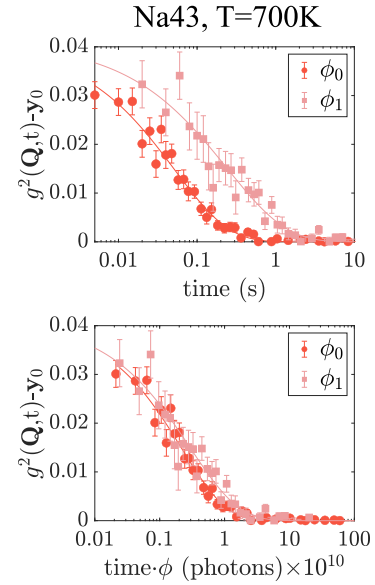

FIG. 5. Dose rate dependence of the dynamics observed in the Na43 sample at 700 K. Upper panel: XPCS curves at two different values of the incident photon flux, $\phi_0 = 4.2 \times 10^{10}$ ph/s and $\phi_1 = 1.2 \times 10^{10}$ ph/s. Lower panel: the same curves plotted as a function of the total incident photons on the sample, a quantity proportional to the absorbed dose.

samples, those with higher sodium content show a lower relative variation of the FSDP and the transformation takes place at lower absorbed doses.

B. Temperature dependence of the dynamics

The temperature dependence of the relaxation time for the Na43 sample is shown in Fig. 4. The black diamonds are the equilibrium values of τ_α, determined from literature data of the frequency dependence of the mechanical loss modulus [33]. These points are well described by a Vogel-Fulcher-Tamman (VFT) model, shown as a dashed line in the figure. The XPCS relaxation time (full blue circles) reaches the macroscopic value of the structural relaxation when the temperature far exceeds T_g, indicating that in the supercooled liquid the dynamics induced by the beam does not affect the relaxation any more. A similar result has been found for the composition with $x = 20\%$ [9]. The observed dynamics is given by the temperature-dependent structural relaxation and the induced one driven by the x-ray beam, and these have been treated in the literature as two independent processes [13,15]. The XPCS relaxation time is obtained by the relation [13,34]

$$\frac{1}{\tau(F,T)} = \frac{1}{\tau_\alpha(T)} + \frac{1}{\tau_{ind}(F)}, \qquad (7)$$

where F is the absorbed photon flux and τ_{ind} a temperature-independent quantity. In the present case, on the contrary, τ_{ind} is temperature dependent in the proximity of T_g. In fact, the application of Eq. (7) with the assumption of a constant value for τ_{ind} gives the continuous line in Fig. 4, which does not follow the XPCS points in the transformation region, so $\tau_{ind} = \tau_{ind}(F,T)$. The temperature dependence of τ_{ind} can be determined by inverting Eq. (7), with the assumption that

τ_α follows the VFT fit. The resulting estimate is plotted in the inset of the figure. Near the glass transition temperature, the beam induced dynamics is affected by the structural rearrangement of the glass and thus it shows a strong temperature dependence in this region. The behavior is compatible with the creation of defects in the glass matrix which is known to be driven by temperature in some oxides [35].

We have confirmed that, up to a temperature of 700 K, the relaxation time is dominated by the induced dynamics by measuring the XPCS curves at two values of the x-ray dose rate. A reduction of the incident photon flux, which is proportional to the dose rate if all the other parameters are fixed, implies a corresponding increase of the observed relaxation time, as shown in the upper panel of Fig. 5. The lower panel of the figure highlights the fact that the curves collapse one onto the other if they are plotted as a function of the absorbed dose.

C. Induced dynamics in the new amorphous state

The irradiated samples are microscopically rearranged by the x-ray beam also after the amorphous transformation has taken place, as shown by the complete decorrelation at long exposure times in the data of Fig. 2. The parameters of the KWW fit to the XPCS curves at room temperature in this regime for the silicate glasses are shown in Fig. 6 at $Q = 1.5$ Å^{-1} as a function of the sodium oxide content. The upper panel shows the absorbed dose corresponding to the XPCS relaxation time, evaluated from Eq. (5). The dose required to completely rearrange the structure decreases monotonically with the increase of the sodium content, indicating that a more floppy network rearranges more easily than a rigid one.

All the correlation curves are stretched, with a β parameter compatible with 1 for $x = 16\%$ and decreasing to 0.5 at
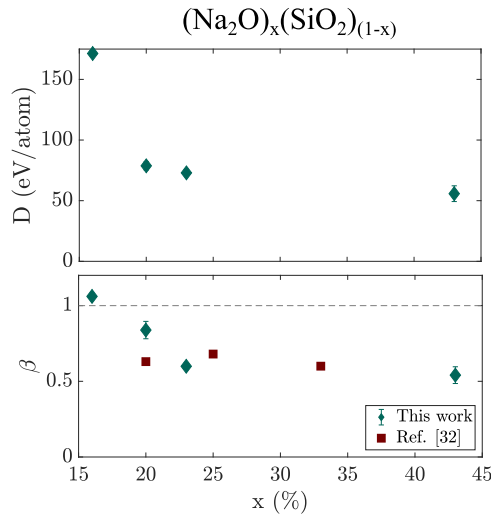
FIG. 6. Upper panel: Absorbed dose in an XPCS relaxation time as a function of the sodium oxide content, measured at room temperature. Bottom panel: β parameter (diamonds). The brown squares are β values determined from macroscopic measurements [33]. The values have been calculated by fitting the loss modulus curve with an Hevriliaki-Negami model [36] and by using the formula given in [37].

elevated Na concentrations, as shown in the bottom panel. More importantly, the β values are similar to those found from macroscopic measurements on the same glasses in the supercooled liquid state (brown squares in the bottom panel). It is, however, important to note that the dynamics investigated here refers to wave vectors around the FSDP maximum while macroscopic measurements probe the dynamics on long distances. The discrepancy between the microscopic and the macroscopic values of β for sample Na20 could be associated to the different probed length scale, as observed in the presence of De Gennes narrowing [38]. These observations suggest that the system is allowed to explore metabasins of the PEL, characterized by a distribution of relaxation times similar to that of the supercooled liquid. The explored local minima of the PEL must correspond to the same average structure, because the diffraction profile is now stable to irradiation. This behavior is compatible with a description in which the transformation to the new amorphous state has rejuvenated the glass, moving it towards a higher energy region in the PEL, as suggested by numerical simulations [8,39]. Our data do not allow us to perform a direct comparison between the diffraction profile of the new amorphous structure with that of the high temperature liquid. We can only note that a decrease and broadening of the FSDP is observed in vitreous silica as the temperature is increased from the glass to the liquid phase and the magnitude of this variation is similar to that of Fig. 3 for the silicate glass with lower sodium content [40].

D. Relationship between radiation dose and network rigidity

In the Cooper and Gupta rigidity theory [26] the number of degrees of freedom per vertex, f, is calculated as the difference between the network dimensionality and the number of
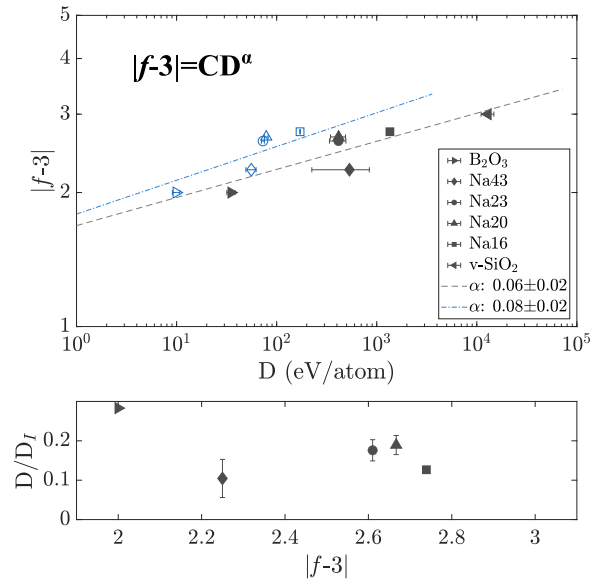

FIG. 7. Top panel: number of constraints per vertex as a function of the absorbed dose for a selection of six glasses. Full symbols (black) refer to the total absorbed dose, D_I, necessary for the structural transformation, a quantity proportional to τ_I. The open symbols (blue) report the value of D, the absorbed dose in one XPCS relaxation time at $Q = 1.5$ Å^{-1}. The SiO$_2$ point is taken from the Supplemental Material of [10]. The dotted lines represent a power-law fit with the exponent α reported in the legend. Bottom panel: ratio of the two doses shown in the upper panel as a function of the number of constraints per vertex.

constraints per vertex: $f = d - h$. Geometrical considerations imply that infinitely large TD networks can exist only if f is non-negative. Regular, congruent, and rigid (RCR) polytopes are identified by two numbers: their dimensionality (δ) and the number of vertices (V). TD networks of vertex sharing RCR polytopes have a number of degrees of freedom per vertex given by the expression

$$f = d - C_{av}\left[\delta - \frac{\delta(\delta + 1)}{2V}\right], \qquad (8)$$

where C_{av} is the average connectivity per vertex. In v-SiO$_2$ the tetrahedron has $\delta = 3$ and $V = 4$. Every vertex connects two tetrahedra so that the connectivity is 2, resulting in $f = 0$, at the boundary between freedom and overconstraint. The boron oxide glass can be considered as a mixture of two types of structural units: BO$_3$ triangles and boroxol (B$_3$O$_6$) rings, both having $\delta = 2$ and $V = 3$ with a connectivity $C = 2$, corresponding to $f = 1$. The silicate glasses of the present study have intermediate values of f, between 0 and 1 [26]. The rigid polytope in this case is the tetrahedron but the connectivity is reduced by the addition of Na, whose effect is the increase in the number of nonbridging oxygens.

The dose dependence of the number of constraints per vertex is reported in Fig. 7. Full symbols refer to the dose required for the transformation to the new amorphous state, while the open symbols are the XPCS relaxation times expressed as the corresponding absorbed radiation dose, and represent the average energy per atom necessary to completely rearrange the structure. We have included the amorphization dose also for

v-SiO$_2$, published in the Supplemental Material of Ref. [10]. For the SiO$_2$ case we have not included the value of D because in the article this quantity has been measured only at low absorbed doses and not in the new amorphous phase. The dose required for the amorphous-amorphous transformation can be well fitted with a power law, as shown in the figure. A similar correlation is well established for ceramic materials exposed to heavy-ion bombardment, where the number of constraints per vertex is typically higher than three, since those materials are crystalline [24]. Our observation extends this relation to the case of glasses irradiated by x-ray beams. Only the silicate sample with $x = 43\%$ lies outside of the trend. However, the structural transformation in this glass is barely visible, with the consequence of a high uncertainty on the dose value. A comparison between the D_I values in the figure and those obtained on ceramic oxides by heavy ion irradiation indicates that the x-ray induced radiolytic process has an efficiency three to four orders of magnitude lower than the knock-on displacement by ions [24]. The lower panel of the figure reports the ratio between the dose necessary for the complete decorrelation at $Q = 1.5$ Å^{-1} and the dose of the structural transformation, showing that the atomic rearrangement in the new amorphous phase requires a dose almost a factor 10 lower than D_I. We want to stress that the values of D refer to the dynamics of the new amorphous state which is generally different from the dynamics of the pristine amorphous system.

IV. CONCLUSIONS

We have monitored the structural transformation of boron oxide and of a series of sodium silicate glasses irradiated by hard x rays. This energy is not sufficient for the direct knock-on displacement of atoms and the primary source of defect creation in the glass matrix is due to the radiolytic process. We observe a temperature dependence of the beam induced dynamics that can be associated to a thermal activation of the defect creation rate in the glass transformation region. The glass structure evolves to a new amorphous phase after the absorption of a sample-dependent dose, which can be quantitatively related to the network rigidity. The new structure is stable under irradiation and has an FSDP less intense than the pristine glass. Similar FSDP variations were observed in previous works [10,13] suggesting that also in those cases the glass was undergoing an amorphous to amorphous transformation and the corresponding XPCS parameters were most probably measured in an intermediate regime. The XPCS technique allows us to monitor the structural rearrangement under irradiation, confirming that the new amorphous state continues to explore the PEL, moving between metabasins with a similar medium range order, and with a stretched exponential relaxation comparable with that of the corresponding supercooled liquid.

[1] L. Berthier and M. D. Ediger, J. Chem. Phys. **153**, 044501 (2020).

[2] A. Leadbetter and A. C. Wright, Phys. Chem. Glasses **18**, 79 (1977).

[3] D. L. Griscom, in *Radiation Effects on Optical Materials*, edited by P. W. Levy, International Society for Optics and Photonics (SPIE, 1985), Vol. 0541, pp. 38–59.

[4] F. W. Clinard, Jr. and L. W. Hobbs, *Modern Problems in Condensed Matter Sciences* (Elsevier, New York, 1986), Vol. 13, pp. 387–471.

[5] R. Egerton, P. Li, and M. Malac, Micron **35**, 399 (2004).

[6] R. E. Schenker and W. G. Oldham, J. Appl. Phys. **82**, 1065 (1997).

[7] G. Buscarino, S. Agnello, F. M. Gelardi, and R. Boscaino, Phys. Rev. B **80**, 094202 (2009).

[8] N. M. Anoop Krishnan, B. Wang, Y. Yu, Y. Le Pape, G. Sant, and M. Bauchy, Phys. Rev. X **7**, 031019 (2017).

[9] B. Ruta, G. Baldi, Y. Chushkin, B. Rufflé, L. Cristofolini, A. Fontana, M. Zanatta, and F. Nazzani, Nat. Commun. **5**, 1 (2014).

[10] B. Ruta, F. Zontone, Y. Chushkin, G. Baldi, G. Pintori, G. Monaco, B. Rufflé, and W. Kob, Sci. Rep. **7**, 3962 (2017).

[11] J. Verwohlt, M. Reiser, L. Randolph, A. Matic, L. A. Medina, A. Madsen, M. Sprung, A. Zozulya, and C. Gutt, Phys. Rev. Lett. **120**, 168001 (2018).

[12] K. Holzweber, C. Tietz, T. M. Fritz, B. Sepiol, and M. Leitner, Phys. Rev. B **100**, 214305 (2019).

[13] G. Pintori, G. Baldi, B. Ruta, and G. Monaco, Phys. Rev. B **99**, 224206 (2019).

[14] F. Dallari, G. Pintori, G. Baldi, A. Martinelli, B. Ruta, M. Sprung, and G. Monaco, Condens. Matter Phys. **22**, 43606 (2019).

[15] A. Martinelli, G. Baldi, F. Dallari, B. Rufflé, F. Zontone, and G. Monaco, Philos. Mag. **100**, 2636 (2020).

[16] C. Moynihan, P. Macedo, C. J. Montrose, P. Gupta, M. DeBolt, J. Dill, B. Dom, P. Drake, A. Easteal *et al.*, Ann. N.Y. Acad. Sci. **279**, 15 (1976).

[17] J. Wu and Q. Jia, Sci. Rep. **6**, 20506 (2016).

[18] L. Cipelletti, S. Manley, R. C. Ball, and D. A. Weitz, Phys. Rev. Lett. **84**, 2275 (2000).

[19] B. Ruta, Y. Chushkin, G. Monaco, L. Cipelletti, E. Pineda, P. Bruna, V. M. Giordano, and M. Gonzalez-Silveira, Phys. Rev. Lett. **109**, 165701 (2012).

[20] B. Ruta, G. Baldi, G. Monaco, and Y. Chushkin, J. Chem. Phys. **138**, 054508 (2013).

[21] M. Bouzid, J. Colombo, L. V. Barbosa, and E. Del Gado, Nat. Commun. **8**, 1 (2017).

[22] J.-P. Bouchaud and E. Pitard, Eur. Phys. J. E **6**, 231 (2001).

[23] G. Pintori, G. Baldi, F. Dallari, A. Martinelli, M. Sprung, and G. Monaco, Phys. Rev. B **105**, 104207 (2022).

[24] L. W. Hobbs, C. E. Jesurum, and B. Berger, *Rigidity Theory and Applications* (Springer Science & Business Media, Berlin, 1999), pp. 191–216.

[25] L. W. Hobbs, J. Non-Cryst. Solids **182**, 27 (1995).

[26] P. K. Gupta, J. Am. Ceram. Soc. **76**, 1088 (1993).

[27] J. C. Phillips, J. Non-Cryst. Solids **34**, 153 (1979).

[28] N. P. Bansal and R. H. Doremus, *Handbook of Glass Properties* (Elsevier, New York, 2013).

[29] B. L. Henke, E. M. Gullikson, and J. C. Davis, At. Data Nucl. Data Tables **54**, 181 (1993).

[30] H. Jabraoui, Y. Vaills, A. Hasnaoui, M. Badawi, and S. Ouaskit, J. Phys. Chem. B **120**, 13193 (2016).

[31] R. L. Owen, J. M. Holton, C. Schulze-Briese, and E. F. Garman, J. Synchrotron Radiat. **16**, 143 (2009).

[32] A. Madsen, A. Fluerasu, and B. Ruta, *Synchrotron Light Sources and Free-Electron Lasers: Accelerator Physics, Instrumentation and Science Applications* (Springer, Cham, 2020).

[33] J. Mills, J. Non-Cryst. Solids **14**, 255 (1974).

[34] Y. Chushkin, J. Synchrotron Radiat. **27**, 1247 (2020).

[35] M. Tomozawa and R. H. Doremus, *Glass I: Interaction with Electromagnetic Radiation: Treatise on Materials Science and Technology* (Elsevier, New York, 2017), Vol. 12, Chap. 7.

[36] S. Havriliak and S. Negami, Polymer **8**, 161 (1967).

[37] F. Alvarez, A. Alegria, and J. Colmenero, Phys. Rev. B **44**, 7306 (1991).

[38] P. G. De Gennes, Physica **25**, 825 (1959).

[39] N. M. Anoop Krishnan, B. Wang, Y. Le Pape, G. Sant, and M. Bauchy, Phys. Rev. Mater. **1**, 053405 (2017).

[40] L. Skinner, C. Benmore, J. Weber, M. Wilding, S. Tumber, and J. Parise, Phys. Chem. Chem. Phys. **15**, 8566 (2013).